

Directional Calibration of Wave Reanalysis Databases using Instrumental Data

R. MÍNGUEZ *, A. ESPEJO , A. TOMÁS , F.J. MÉNDEZ AND I.J. LOSADA

Environmental Hydraulics Institute “IH Cantabria”, Universidad de Cantabria, Spain

* *Corresponding author address:* Roberto Mínguez, Environmental Hydraulics Institute “IH Cantabria”,
Universidad de Cantabria, Spain.

E-mail: roberto.minguez@unican.es

ABSTRACT

Wave reanalysis data bases (WRDB) offer important advantages for the statistical characterization of wave climate (continuous time series, good spatial coverage, constant time span, homogeneous forcing, more than 40 year-long time series) and for this reason, they have become a powerful tool for the design of offshore and coastal structures. However, WRDB are not quantitatively perfect and corrections using instrumental observations must be addressed before it is used, this process is called calibration. The calibration is specially relevant near the coast and in areas where the orography is complex, since in these places the inaccuracy of WRDB is evident due to the bad description of the wind fields, i.e. insufficient forcing resolution. The quantitative differences between numerical and instrumental data suggests that different corrections should be applied depending on the mean direction of the sea state. This paper proposes a calibration method based on a nonlinear regression problem where the corresponding correction parameters vary smoothly along the possible wave directions by means of cubic splines. The correction of significant wave height is performed using instrumental data: i) buoy records and/or ii) satellite data. The performance of the method is illustrated considering data from different locations around Spain.

1. Introduction

In the last years, the development of wave reanalysis models allow a detailed description of wave climate in locations where long-term buoy records are not available. For this reason they have become a powerful tool used for the design of offshore and coastal structures, since they provide long continuous time series records with good spatial coverage. However, reanalysis models are simplifications of reality which also use discrete forcing fields consisting of surface winds at different times, and quantitative results present differences when comparing with recent instrumental data (buoys and/or satellite) (see Caires and Sterl (2005) and Cavaleri and Sclavo (2006)). Cavaleri and Bertotti (2004) pointed out that when the orography is complex, the reanalysis inaccuracy becomes more evident due to the bad description of wind fields, which does not have the appropriate spatial and temporal resolution.

The definition of the wave climate is crucial for coastal management and design, and there has been an increased interest in collecting information through instrumental devices, mainly using buoys and satellite altimetry. Buoys provide time series records of different ocean climate variables such as significant wave height, wave direction, wave period, currents, wind direction, etc. depending on the type of device. This information is very valuable for coastal design, however it is only valid for the buoy location and in most cases the time series have interruptions due to disruptions on the normal use caused by buoy failure. From the seventies, several satellite missions (Skylab, Geos-3, Seasat, Geosat, Topex/Poseidon, Ers-1, Ers-2, Gfo, Jason-1, Envisat, and Jason-2) incorporate altimetry sensors which allows the evaluation of different ocean climate variables, such as significant wave height with a high level of precision (± 3 cm, Krogstad and Barstow (1999)). Altimetry data consist of

information about significant wave height, among others variables, at different locations and time frames. However, with these two sources of information: buoys and altimetry, we do not have a temporal and spatial homogeneous record of ocean wave climate variables for design purposes. This reason has motivated an increased interest in the development of different wave generation models such as WAM (see Hasselman et al. (1988)), which using wind fields as input data, try to reproduce the evolution of wave generation and propagation on an homogeneous framework, both in time and space. These wind wave numerical databases provide continuous records of significant wave height, mean period and mean direction, which are the key parameters for wave climate characterization, on a regular time basis (hourly or 3-hourly) over a defined grid. This information set has the advantages of both buoy and altimetry data, i.e. homogeneous spatial and temporal characteristics, however, as it has been pointed out by several authors, results are subject to bias with respect to instrumental data. Cavaleri and Sclavo (2006) summarized the main characteristics of these sources of information as follows:

Buoys: accurate, frequent (typically at 3-h intervals), but limited in number, very sparse and mostly close to coasts,

Satellites: good accuracy, except for very low and high values, continuous, but very intermittent at a given location, difficulties in working close to coast,

Numerical models continuous in space and time, full information (wave spectrum), but often underestimated in the enclosed basins.

Note that wave hindcasting usually refers to a numerical model integration over a historical period without assimilating observations, since oceanographic observations such as the

significant wave height are much scarcer than meteorological observations, and it has been considered adequate for generating a reasonable representation of wave climate with little need for a full reanalysis. On the other hand, reanalysis models incorporate observational information within the process. Note that the term “wave reanalysis” is usually adopted in the wave climate scientific community to indicate that it is forced by a wind atmospheric reanalysis which assimilates observations. For this reason we prefer to use the term “reanalysis ” instead of “hindcast” Thus, data for the case studies presented, properly speaking, come from hindcast models without assimilating instrumental observations.

Since the three sources of information have advantages and drawbacks, several attempts to combine this information have been presented in the literature. Caires and Sterl (2005) proposed a nonparametric method to correct model data. At any given point in space and time the correction is determined from analogs in a learning dataset. This dataset contains model data and simultaneous observations and it is applied to the significant wave height dataset of the 45-yr European Centre for Medium-Range Weather Forecasts Re-Analysis (ERA-40). Cavaleri and Sclavo (2006) made use of the overall information on models, buoys and satellite to obtain calibrated decadal time series at a large number of points, distributed at 0.5° intervals in the Mediterranean Sea. These two approaches are applied on a point-to-point basis without considering either the spatial correlation between neighbor nodes or the wave direction. In an attempt to include spatial correlation in the calibration procedure, Tomás et al. (2008) proposed a spatial calibration procedure based on empirical orthogonal functions and a non-linear transformation of the spatial-time modes. However, the method proposed by Tomás et al. (2008) assumes a prior distribution function of the data all around the study area which may not be valid for certain cases, and it is suitable for global hindcast

datasets.

Due to the characteristics of reanalysis models, which are primarily fed using wind data, it is known that inaccuracies of WRDB are mostly dependent on the bad description of the wind fields (see Feng et al. (2006)), i.e. insufficient forcing resolution. In coastal areas, there are additional factors that contribute to poor model performance, such as, inappropriate shallow water physics in wave models, unresolved island blocking, imperfect bathymetry, etc. (see Cavaleri et al. (2007) for a summary). The quantitative differences between numerical and instrumental data suggests that different corrections should be applied depending on the mean direction of the sea state, i.e. for directions where the wind resolution is not enough to capture the local wind wave generation, but not for swell waves generated in areas where the wind resolution is sufficient to reproduce the wave dynamics. Tomás (2009) proposes a calibration method where the parameters depend on the wave direction using harmonic functions. Mackay et al. (2010a,b) also point out the necessity of hindcast calibration in the context of wind energy resource assessment.

The aim of this paper is to present a new parametric calibration method based on a nonlinear regression problem with the following characteristics:

- i. It manages to combine buoy, satellite and model data.
- ii. The correction parameters vary smoothly along the possible mean wave directions by means of cubic splines, allowing different corrections depending on the wave direction.
- iii. Corrections are made on empirical quantile information on a Gumbel probability paper scale. This allows to give more weight on the calibration procedure to the maximum data, which is more important from the design point of view.

iv. Classical regression theory is applied to the calculation of the confidence intervals for parameters estimates and corrected values, giving an idea of the uncertainty associated with the calibration process.

The paper is organized as follows. In Section 2, we present the nonlinear regression problem to be used for calibration purposes, analyzing in detail how the parameters are modeled via spline functions and it describes the complete calibration methodology including the diagnostic analysis and uncertainty characterization. Section 3 illustrates the functioning of the method through several examples on different locations around Spain, and in Section 4 the effect of directional uncertainty on those locations is analyzed. Finally, in Section 5 relevant conclusions are duly drawn.

2. Nonlinear regression model

The intrinsically (nonlinearizable) nonlinear regression model can be written as

$$y_i = f(\mathbf{x}_i; \boldsymbol{\beta}) + \varepsilon_i, \quad i = 1, 2, \dots, n_d, \quad (1)$$

where y_i is the i th value of the response variable, \mathbf{x}_i is a $k \times 1$ vector of predictor variables corresponding to the i th observation, and ε_i is a random error. The function f is known and nonlinear in the parameter vector $\boldsymbol{\beta}$. The most popular method for estimating the regression parameters $\boldsymbol{\beta}$ is the least squares (LS) method, where we minimize the sum of squared distances between observed and predicted values, that is,

$$\underset{\boldsymbol{\beta}}{\text{Minimize}} \quad Z_{LS} = \boldsymbol{\varepsilon}^T \boldsymbol{\varepsilon} = \sum_{i=1}^{n_d} (y_i - f(\mathbf{x}_i; \boldsymbol{\beta}))^2, \quad (2)$$

where ε are the residuals, which are assumed to be uncorrelated and identically distributed normal random variables with zero mean and unknown constant variance, and n_d is the number of observations.

For the calibration process, we consider that response and predictor variables correspond to instrumental significant wave heights (buoy and satellite, H_s^I) and reanalysis significant wave heights (H_s^R), respectively. The nonlinear function f is equal to:

$$f(\mathbf{x}; \boldsymbol{\beta}) = f(a^R, b^R; H_s^R, \theta) = a^R(\theta) [H_s^R]^{b^R(\theta)} = H_s^C, \quad (3)$$

where H_s^R is the reanalysis significant wave height, H_s^C is the calibrated or corrected significant wave height, and $a^R(\theta)$ and $b^R(\theta)$ are the parameters dependent on the wave direction θ . Note that although we particularize equations for significant wave height variables, the method is also valid for other reanalysis variables such as wind velocity or mean wave periods.

The model relies on the assumption that parameters a^R and b^R vary smoothly with the propagation direction (θ). These variations are introduced in the model throughout cubic splines, so that only a given number n_p of values of the parameters at different given directions $a_j, b_j; j = 1, \dots, n_p$ are known (see the circle points in Figure 1 (a)). The parameter values for all possible directions are obtained interpolating through smoothing cubic spline functions as follows:

$$a_i^R(\theta_i) = a_j + x_j^a(\theta_i - \theta_j) + y_j^a(\theta_i - \theta_j)^2 + z_j^a(\theta_i - \theta_j)^3, \quad (4)$$

$$b_i^R(\theta_i) = b_j + x_j^b(\theta_i - \theta_j) + y_j^b(\theta_i - \theta_j)^2 + z_j^b(\theta_i - \theta_j)^3, \quad (5)$$

where a_i^R and b_i^R are the interpolated model correction parameters for a given direction θ_i , $a_j, b_j; j = 1, \dots, n_p$ are the parameters to be estimated, i.e. the parameter values

associated with directions θ_j ; $j = 1, \dots, n_d$, and $x_j^a, y_j^a, z_j^a, x_j^b, y_j^b, z_j^b$; $j = 1, \dots, n_d$ are the corresponding cubic spline parameters, which are obtained using zero, first and second order continuity conditions along the circumference ($0 \leq \theta \leq 2\pi$). Note in Figure 1 that distances h_j between direction locations do not need to be equally spaced. Additionally, from the practical point of view $\theta_1 = 0$ and $\theta_{n_p+1} = 2\pi$, which corresponds with the same direction (angle) value, and for this reason, the following conditions must be fulfilled:

$$\begin{aligned} a_1 &= a_{n_p+1} \\ b_1 &= b_{n_p+1}, \end{aligned} \tag{6}$$

this is the reason why only n_p parameters have to be considered for the spline definition.

Under these considerations and using equation (2) the spline parameters a_j, b_j ; $j = 1, \dots, n_p$ estimation consist of determining the optimal values by solving the following optimization problem:

$$\begin{aligned} \text{Minimize} \quad & \sum_{i=1}^{n_d} (H_{s_i}^I - H_{s_i}^C)^2 = \sum_{i=1}^{n_d} \left(H_{s_i}^I - a_i^R(\theta_i) [H_{s_i}^R]^{b_i^R(\theta_i)} \right)^2 \\ & \mathbf{a}, \mathbf{b} \end{aligned} \tag{7}$$

subject to

$$\left. \begin{aligned} a_i^R &= a_j + x_j^a(\theta_i - \theta_j) + y_j^a(\theta_i - \theta_j)^2 + z_j^a(\theta_i - \theta_j)^3 \\ b_i^R &= b_j + x_j^b(\theta_i - \theta_j) + y_j^b(\theta_i - \theta_j)^2 + z_j^b(\theta_i - \theta_j)^3 \end{aligned} \right\} \quad i = 1, \dots, n_d, \tag{8}$$

$$a_j > 0; \quad j = 1, \dots, n_p \tag{9}$$

$$\mathbf{g}(\mathbf{a}, \mathbf{b}) = \mathbf{0} \tag{10}$$

where n_d is the number of data pairs (H_s^I, H_s^R) available for parameter estimation. Note also that each data pair uses a different cubic polynomial depending on the direction values according to the following condition $\theta_j \leq \theta_i < \theta_{j+1}$. This does not represent a problem from

the practical point of view because both the values $\theta_j; j = 1, \dots, n_p$ and $\theta_i; i = 1, \dots, n_d$ are data for the estimation procedure. Constraint (9) ensures positiveness of parameters \mathbf{a} , since significant wave height must remain positive. Constraint (10) represents all required equations for the definition of the cubic spline parameters $x_j^a, y_j^a, z_j^a, x_j^b, y_j^b, z_j^b; j = 1, \dots, n_p$. A detailed definition of these equations is given in an Appendix.

Observe that, from a mathematical point of view, the problem defined in Equations (7)-(10) consists of the minimization of a positive sum of continuously derivable convex functions defined on a compact set, i.e. a convex function with linear constraints. Hence, there exists one and only one solution provided that constraints are feasible, which it is the case for the cubic spline definition. The minimization problem can be solved using any of the available solvers for nonlinear programming subject to linear constraints, such as MINOS (Murtagh and Saunders 1998) under GAMS (Brooke et al. 1998), which also allows including bounds on parameters to be estimated. The method uses a reduced-gradient algorithm (Wolfe 1963) combined with the quasi-Newton algorithm described in Murtagh and Saunders (1978) where the gradient vector information is obtained using numerical differentiation. Alternatively, the optimization procedure can be solved using the sequential quadratic programming (SQP) method, where the estimate of the Hessian of the Lagrangian at each iteration is computed using the BFGS formula (see Powell (1978)).

In the previous section the nonlinear model proposed for parameter estimation of the calibration method was presented. However, the calibration procedure as a whole, i.e the obtention of the final calibrated time series in a particular location, involves several additional steps:

- i. *Data and quantile selection.* The calibration procedure is intended to correct the probability distribution function of the reanalysis variable in order to be as close as possible to the instrumental variable probability distribution. For this task, it is required to use both reanalysis and instrumental data coincident in time and space, and the selection of the appropriate quantiles to be compared.
- ii. *Smooth quantile calculation.* Since the calibration procedure assumes a smooth variation of the calibration parameters, the selected quantiles for different directions must be calculated.
- iii. *Parameter estimation.* Using the reanalysis and instrumental quantiles, the parameters are estimated solving the problem (7)-(10).
- iv. *Diagnostic analysis.* Confidence intervals of the parameters to measure the quality of the calibration procedure are estimated using classical regression techniques.
- v. *Time series calibration.* Once the optimal calibration parameters are available, it is possible to correct the reanalysis time series related to a given location.
- vi. *Diagnostic time series analysis calibration.* Using also standard regression techniques, confidence intervals for the calibrated time series are calculated. This diagnostic allows quantifying the uncertainty associated with the calibration procedure. Several diagnostic plots are also listed.

All the aforementioned steps are explained in detail in the following subsections.

a. *Data and quantile selection*

The target of the calibration procedure is to correct the significant wave height reanalysis time series record at a particular location (see the objective point in Figure 2) using instrumental data. For this purpose, the first step of the method is to select n_d data pairs (H_s^I, H_s^R) in an area close to the objective point where the wave climate is similar. The definition of an automatic criterion to select the data to be incorporated for the posterior parameter estimation procedure is difficult, however we propose a procedure based on vectorial correlation (Crosby et al. 2003), sensitivity tests (Tomás 2009) and designer criterion. The guidelines for *data selection* are summarized as follows:

- i. Select a circular area around the objective point of radius r (*neighborhood criterion*).

The length of the radius depends on the ocean climate homogeneity and the number of available data. There must be a compromise between the data record length and its homogeneity, since the longer the radius the higher the length of the record but it is more likely to use data with different wave climate. In our experience and after several sensitivity tests using different parameter configurations around the Spanish coast, we derived the following rule of thumb: i) $r = 0.5^\circ$ for complex areas such as Mediterranean sea; ii) $r = 1^\circ$ for Atlantic ocean coastlines, and iii) $r = 2^\circ$ for open areas.

- ii. The homogeneity criterion is further supported using the concept of vector correlation (Crosby et al. 2003), which is a generalization of the standard scalar correlation coefficient including both directional and magnitude information. Vector correlation is equal to zero when the vectors are independent and obtains its maximum value (2

for the two dimensional case) if and only if they are linearly dependent. Thus, from different tests performed, data within the *neighborhood criterion* circle whose vector correlation is higher than 1.5 are taken for calibration purposes, otherwise they are removed.

- iii. In shallow water areas and depending on the spatial resolution of wave reanalysis, it might be necessary to consider data pairs with relative water depth h/L similar to or larger than that at the objective location, where h and L are water depth and wave length, respectively. This aspect is very important in order to avoid possible bias in the direction of the wave reanalysis, which may not be adequately reproduced by the wave propagation model if the spatial resolution is coarse, i.e. more than 25 km. Nevertheless, the proposed procedure is robust with respect to directional calibration bias, as shown in Section 4.
- iv. When the orography is complex and dealing with significant wave height, as the case shown in Figure 2 (b), in order to avoid using diffracted or sheltered wave data whose wave climate may be very different from the one in the objective location, a *ray criterion* is used, i.e. only data within the circle so that, if the line joining its location with the objective point does not intercept land, is taken into consideration, as shown in Figure 2 (b). Note that diffracted data may present a high vector correlation if directions and magnitudes are affected by a constant, but we rather not to consider them.
- v. Once the locations of the data to be considered are defined and for comparisons to be meaningful, both reanalysis and instrumental data pairs coincident in location and time must be obtained. This process is performed interpolating spatially and temporally

the reanalysis data. The final result is a set of n_d data pairs (H_s^I, H_s^R) which are used afterwards for quantile calculations.

Note that the selection criteria are based on previous results, heuristic guidelines from sensitivity tests and under certain assumptions. Computational performance tests have shown that the methodology provides satisfactory results for the locations studied (Mediterranean Sea and Atlantic Ocean). Nevertheless, further research must be done about the data selection criteria considering that this data should have homogeneous calibration parameters for other locations around the world.

The selected n_d pairs (H_s^I, H_s^R) would allow us to get calibration parameter estimates solving the problem (7)-(10). However, since most of the data are in the medium and lower parts of the distribution, this would produce a masking effect for the highest significant wave heights, which would not receive the appropriate correction. To avoid this shortcoming a quantile calibration is proposed, instead of using n_d data pairs, quantiles associated with a given number n_q of probabilities on a Gumbel scale are chosen as follows:

$$q_{lo} = -\log(-\log(1/n_d)) \quad (11)$$

$$q_{up} = -\log(-\log(1 - 5/n_d)) \quad (12)$$

$$x_{q_i} = q_{lo} + (i - 1) \frac{q_{up} - q_{lo}}{n_q}; \quad i = 1, \dots, n_q, \quad (13)$$

$$q_i = \exp(-\exp(-x_{q_i})); \quad i = 1, \dots, n_q, \quad (14)$$

where q_{lo} and q_{up} are the Gumbel scale values associated with the lower $(1/n_d)$ and higher $(1 - 5/n_d)$ probabilities, respectively, $x_{q_i}; i = 1, \dots, n_q$ are equally space values on the Gumbel scale, and $q_i; i = 1, \dots, n_q$ are the corresponding quantile probabilities. For instance, if $n_d = 1000$ and $n_q = 5$, then the quantiles result in $q = \{0.0010, 0.3218, 0.8302, 0.9699, 0.9950\}$,

where three of them belong to the higher tail of the distribution.

b. Smooth quantile calculation

In the previous step, a set of n_d data pairs (H_s^I, H_s^R) and different quantile probabilities q were determined. Next step encompasses the evaluation of the selected quantiles associated with the probabilities q from the H_s^I and H_s^R empirical distribution functions, respectively, so that the calibration parameter estimation is performed using quantile pairs $(q_{H_s^I}^I, q_{H_s^R}^R)$ instead of data pairs. Since the proposed calibration technique introduces smooth variations depending on wave direction, the quantile calculation requires to embed somehow the wave direction information θ . The process works as follows:

- i. First of all a sector with amplitude $\Delta\theta$ must be defined. For practical cases we use $\Delta\theta = \frac{\pi}{8} = 22.5^\circ$, this sector would be a moving sector which will rotate all around the circumference one degree at a time, as shown in Figure 3 (a). At every position of this sector defined by its mean direction θ_i , all data whose direction is within this sector, i.e. $\forall k | \theta_i - \Delta\theta/2 \leq \theta_k \leq \theta_i + \Delta\theta/2$, are chosen as sector data. The selection of $\Delta\theta = 22.5^\circ$ is based on numerical tests, this value provides an smoothing effect which minimizes possible directional bias. Note that defining these corrections based on mean direction θ_i may be a problem for those cases where there are multiple swell and sea components, and although the mean direction is an appropriate representative of the most energetic waves, further research should be done on this particular issue.
- ii. For each sector $i = 1, \dots, 360$, the n_q quantiles $(q_{H_s^I, i}^I, q_{H_s^R, i}^R)$ are obtained using the empirical distribution function of the sector data as shown in Figure 3 (b). For this

task, those quantiles are computed as follows:

- (a) The sorted values in $H_{s,i}^I$ are taken as the $(0.5/n_i^I, 1.5/n_i^I, \dots, [n_i^I - 0.5]/n_i^I)$ quantiles, where n_i^I corresponds to the number of instrumental data within sector i .
- (b) Quantiles associated with probabilities between $(0.5/n_i^I)$ and $([n_i^I - 0.5]/n_i^I)$ are computed using linear interpolation.
- (c) The minimum or maximum values in $H_{s,i}^I$ are assigned to quantiles for probabilities outside that range.

The process is analogous for quantiles related to $H_{s,i}^R$.

Note that at the end of the process there are $n_{dq} = 360 \times n_q$ quantile pairs which can be used for parameter estimation.

There are several computational issues which are important from the practical point of view:

- i. For each sector, there is a minimum number of points in order to calculate empirical quantiles, for instance, the minimum between 5 times the number of quantiles ($5n_q$) and 10% of the number of data pairs ($0.1n_d$). If the number of points within any sector is lower than this quantity, no quantiles are calculated.

- ii. Once the procedure concludes there could exist sectors where no quantiles are available.

This may cause computational convergence problems on the parameter estimation procedure. For this reason, auxiliary quantiles are synthetically generated using linear interpolation between quantiles from adjacent sectors. Note that this result does not

affect the calibration procedure because no data or very low number of points have wave directions within those empty sectors.

iii. The proposed method relies on wave reanalysis derived directional data. It is already known that in nearshore areas, directional bias between reanalysis and directional buoy data is commonly about 10 degrees and can be as much as 40 degrees (e.g., Hemer et al. (2010)). However, we overlook these biases completely for several reasons:

- (a) In some cases, instrumental data do not contain directional information.
- (b) The selection of the window $\Delta\theta$ attenuates possible biases on directional information providing a smoothing effect. Numerical tests have demonstrated that the selection $\Delta\theta = \frac{\pi}{8} = 22.5^\circ$ minimizes the directional biases influence.

For the cases where reanalysis and instrumental directional information is available, it is more efficient to calibrate this information, and use calibrated directional information within the proposed methodology. Including the directional uncertainty in the proposed model is a subject for further research.

c. Parameter estimation

Using the n_{dq} quantile pairs related to reanalysis and instrumental data $(q_{H_s}^I, q_{H_s}^R)$, the solution of problem (7)–(10) provides the optimal estimation parameters $\hat{\mathbf{a}}, \hat{\mathbf{b}}$ of both spline functions.

The minimization of the least squares objective function can be done using nonlinear optimization routines. Nevertheless, from previous experiences, the following comments and

recommendations are pertinent:

- i. Although the parameter estimation problem is an unconstrained minimization problem with respect to the parameter estimation variables, we rather use a constrained optimization solver including parameter bounds, which makes the estimation more robust. These bounds help avoiding parameters \mathbf{a} taking negative values, i.e. $a_j > 0$; $j = 1, \dots, n_p$, which corresponds to physically infeasible corrections on the calibration procedure.
- ii. All Newton-type routines require the user to supply starting values, but the importance of good starting values can be overemphasized. Thus, for the first iteration, initial guesses are taken as:

$$a_j = 1; b_j = 1; j = 1, \dots, n_p, \quad (15)$$

which corresponds to no correction for reanalysis data in the calibration process.

d. Diagnostic analysis

The solution of problem (7)–(10) provides the mean values of the estimated parameters $\hat{\boldsymbol{\beta}}$, and assuming that observational errors are normally distributed, the estimated parameter vector is distributed as follows:

$$\boldsymbol{\beta} \sim N(\hat{\boldsymbol{\beta}}, \Sigma_{\boldsymbol{\beta}}), \quad (16)$$

where N denotes the multivariate normal distribution, and $\Sigma_{\boldsymbol{\beta}}$ is the variance-covariance matrix of the parameter estimates.

One advantage of using least squares method for parameter estimation is that the solution

corresponds to the maximum likelihood estimate. Note that the log-likelihood function for the $\boldsymbol{\varepsilon}$ independent and normally distributed errors is:

$$\ell(\boldsymbol{\beta}, \sigma^2) = -\frac{n_{dp}}{2} \log(2\pi\sigma^2) - \frac{1}{2\sigma^2} \left[\sum_{i=1}^{n_{dp}} (y_i - f(\mathbf{x}_i; \boldsymbol{\beta}))^2 \right]. \quad (17)$$

Once the parameters of the regression model are estimated it is also of interest the *error mean square* or *residual variance* $\hat{\sigma}^2$, whose unbiased estimator is:

$$\hat{\sigma}^2 = \frac{\sum_{i=1}^{n_{dp}} (y_i - f(\mathbf{x}_i; \boldsymbol{\beta}))^2}{n_{dp} - n_p - 1}. \quad (18)$$

Using the method of maximum likelihood, if $\ell(\boldsymbol{\beta}, \sigma^2)$ is twice differentiable with respect to estimated parameters, and under certain regularity conditions which are often satisfied in practice (Lehmann and Casella (1998)). The parameters covariance matrix is equal to the inverse of the *Fisher information matrix* ($\mathbf{I}_{\boldsymbol{\beta}}$), which is equal to the Hessian matrix of the log-likelihood function with the sign changed:

$$\mathbf{I}_{\boldsymbol{\beta}} = -\frac{\partial^2 \ell(\boldsymbol{\beta}, \sigma^2)}{\partial^2 \boldsymbol{\beta}}. \quad (19)$$

Considering (2) and (17) the *Fisher information matrix* in (19) can be rewritten as:

$$\mathbf{I}_{\boldsymbol{\beta}} = \frac{1}{2\hat{\sigma}^2} \frac{\partial^2 (\boldsymbol{\varepsilon}^T \boldsymbol{\varepsilon})}{\partial^2 \boldsymbol{\beta}} = \frac{\mathbf{H}_{\boldsymbol{\beta}}}{2\hat{\sigma}^2}, \quad (20)$$

where $\mathbf{H}_{\boldsymbol{\beta}}$ is the hessian of the least square objective function, which can be obtained numerically by finite differences or, depending on the optimization algorithm used, can be a subproduct of the optimization procedure. The corresponding inverse is the variance-covariance matrix:

$$\boldsymbol{\Sigma}_{\boldsymbol{\beta}} = \mathbf{I}_{\boldsymbol{\beta}}^{-1}. \quad (21)$$

The $(1 - \alpha)$ confidence interval for each parameter is equal to:

$$\begin{aligned}\beta_j^{\text{up}} &= \hat{\beta}_j + t_{(1-\alpha/2, n_{dp}-n_p-1)} \hat{\sigma}_j, \quad j = 0, 1, \dots, n_p \\ \beta_j^{\text{lo}} &= \hat{\beta}_j - t_{(1-\alpha/2, n_{dp}-n_p-1)} \hat{\sigma}_j, \quad j = 0, 1, \dots, n_p,\end{aligned}\tag{22}$$

where $t_{(1-\alpha/2, n_{dp}-n_p-1)}$ is the Student's t -distribution $(1 - \alpha/2)$ quantile with $n_{dp} - n_p - 1$ degrees of freedom and $\hat{\sigma}_j$ is the estimated standard deviation for parameter j (square root of the corresponding diagonal term in $\Sigma\boldsymbol{\beta}$).

e. Time series calibration

Once the optimal calibration parameters $\hat{\mathbf{a}}$ and $\hat{\mathbf{b}}$ are available, it is possible to correct the reanalysis time series related to a given location given the pairs $(\theta_i, H_{s_i}^R); \forall i$. The process has two steps:

- i. Obtain the corresponding spline interpolated values \mathbf{a}^R and \mathbf{b}^R using the wave direction information $\boldsymbol{\theta}$ and the estimated spline parameters $\hat{\mathbf{a}}$ and $\hat{\mathbf{b}}$.
- ii. The application of the correction (3) for each data:

$$H_{s_i}^C = a_i^R(\theta_i) [H_{s_i}^R]^{b_i^R(\theta_i)}; \forall i,\tag{23}$$

where $H_{s_i}^C; \forall i$ is the calibrated data.

Note that this step is also affected by the effect of directional bias. However, it has been numerically tested that the relative sensitivity of the calibrated data $H_{s_i}^C$ with respect to θ_i is considerably lower than w.r.t $H_{s_i}^R$. This justifies the good performance of the proposed method. The inclusion of this bias could enhance results and is a subject for further research.

f. Diagnostic time series analysis calibration

Analogously to the parameter estimation process, and considering that spline calibration parameters $\boldsymbol{\beta} = (\mathbf{a}; \mathbf{b})^T$ follow a multinormal distribution with parameters $\hat{\boldsymbol{\beta}}$ and $\Sigma_{\boldsymbol{\beta}}$. Then for a large sample size n_{dp} , the corrected significant wave height $H_{s_i}^C$ is asymptotically normal, that is,

$$H_{s_i}^C \sim N(\hat{H}_{s_i}^C, \nabla_{\boldsymbol{\beta}}^T H_{s_i}^C \Sigma_{\boldsymbol{\beta}} \nabla_{\boldsymbol{\beta}} H_{s_i}^C); \quad i = 1, \dots, n_d, \quad (24)$$

where $\nabla_{\boldsymbol{\beta}} H_{s_i}^C$ is the n vector of partial derivatives of $H_{s_i}^C$ with respect to $\boldsymbol{\beta}$, which is given by

$$\nabla_{\boldsymbol{\beta}} H_{s_i}^C = \left[\frac{\partial H_{s_i}^C}{\partial a_1} \quad \dots \quad \frac{\partial H_{s_i}^C}{\partial a_n} \quad \frac{\partial H_{s_i}^C}{\partial b_1} \quad \dots \quad \frac{\partial H_{s_i}^C}{\partial b_n} \right]^T. \quad (25)$$

Note that equation (24) allows obtaining the variance $\sigma_{H_{s_i}^C}^2$ of the corrected significant wave height due to the regression model. If the uncertainty not explained by the regression model wants to be included, the corrected significant wave height intervals are:

$$H_{s_i}^C \pm t_{(1-\alpha/2, n-p-1)} \sqrt{\hat{\sigma}^2 + \sigma_{H_{s_i}^C}^2}; \quad i = 1, \dots, n_d. \quad (26)$$

Besides confidence intervals, it is also interesting the use of different diagnostic statistics for comparing the similarity on the distributions of both reanalysis and calibrated data (y) with respect to instrumental data (x), which is taken as a benchmark:

- The systematic deviation between two random variables (BIAS):

$$\text{BIAS} = \bar{x} - \bar{y}. \quad (27)$$

- The root mean square error (RMS):

$$\text{RMS} = \sqrt{\frac{1}{n_d} \sum_{i=1}^{n_d} (x_i - y_i)^2}. \quad (28)$$

- Residual Scatter Index (RSI), which measures dispersion with respect the line $x = y$:

$$\text{RSI} = \frac{\text{RMS}}{\bar{x}}. \quad (29)$$

- The Pearson's correlation coefficient (ρ).
- Sample distribution moments: mean (μ), standard deviation (σ), skewness (γ), and kurtosis (ξ).

Note that for the first three statistics the lower the value is, the better the agreement between instrumental and reanalysis or calibrated data is. However, it is the opposite for the Pearson's correlation coefficient. These statistics are used to measure the quality of the calibration process comparing the statistics obtained using instrumental-reanalysis versus instrumental-calibrated data.

There are also diagnostic plots such as quantile scatter plots, data scatter plots, empirical distribution function plots for instrumental, reanalysis and calibrated data, which can be used to have a qualitative idea of the goodness of the calibration process.

3. Case study

In this work, we use the reanalysis data base SIMAR-44 generated by Puertos del Estado. For this purpose they used the 44-year (1958-2001) dynamic downscaling REMO (Jacob et al. (2001)) from the global atmospheric re-analysis carried out by the National Centre for Environmental Prediction, Washington, USA (NCEP) and the National Centre for Atmospheric Research, Boulder, Colorado, USA (NCAR) and the wave model WAM

(Hasselmann et al. (1988))). This SIMAR-44 reanalysis consist on hourly time series over a 44-year period (1958-2001) of significant wave height (H_s), mean period (\bar{T}) and mean direction (θ) over different regular grids around Spain.

We have selected two different locations to apply the calibration methodology: i) Cabo de Gata, and ii) Estaca de Bares, as shown in Figure 4. We have selected reanalysis nodes on these locations because there are available instrumental data consisting of buoy records from Puertos del Estado network and altimeter information from five different satellite missions: TOPEX, TOPEX 2, Jason, Envisat, and Geosat Follow-On (GFO). These data are given over different time frames.

Wave climate at “Cabo de Gata” location has two predominant wave directions, E-ENE and W-WSW corresponding to waves coming from the Mediterranean sea (levantes) and Atlantic Ocean (ponientes), respectively, as shown in Figure 5 (a). Note that in this location the effect of wave directionality is very important. Wave climate at “Estaca de Bares” location is more homogeneous in direction (see Figure 5 (b)), where swell waves from the North West are predominant. In Figure 6 it is shown a comparison between the significant wave height (SWH) at the Cabo the Gata buoy and the reanalysis for year 2000. Note that the agreement is satisfactory reinforcing the hypothesis of using WRDB to define wave climate at any specific location at the coast, however there are still discrepancies which may be important for design purposes.

We have applied the calibration methodology for both locations following the steps in Section 2:

- i. *Data and quantile selection.* We take as data both buoy and satellite records around

the specific locations in a ratio of 1° for Estaca de Bares and 0.5° for Cabo de Gata, as shown in Figure 4. Note that all data within those circles have a vector correlation higher than 1.5.

ii. *Smooth quantile calculation.* The number of quantiles and sector width is $n_q = 20$ and $\Delta\theta = \frac{\pi}{8} = 22.5^\circ$, respectively. In Figure 7, the selected quantiles for different directions are shown. Each quantile is plotted on a different gray scale color to facilitate quantile recognition all over the circumference. Note that upper graphs correspond to reanalysis quantiles, and below graphs are the corresponding instrumental (buoy and satellite) quantiles. These will be used in the parameter estimation procedure. In both cases there are directions where no data exist, for this reason, there are synthetically generated smooth quantiles using linear interpolation.

iii. *Parameter estimation.* Using the reanalysis and instrumental quantiles, the parameters are estimated solving the problem (7)-(10). The optimal values are provided in Table 1. Their evolution is also shown in Figure 8. Note from these results that reanalysis for Estaca de Bares location, where wave climate is the response to the wind fields in the entire NE Atlantic, provides satisfactory results, being the calibration parameters on the main directions very close to one. This corresponds to no correction. However, the reanalysis of Cabo de Gata is deficient due to the low wind spatial resolution on the Mediterranean sea.

iv. *Diagnostic analysis.* Confidence intervals of the parameters are estimated using classical regression techniques, which are provided in Table 1 and shown in Figure 8. In Figure 9 it is also shown the cumulative distribution function of instrumental, reanaly-

sis and calibrated quantiles. Note that the calibrated quantile probability distribution presents good agreement with instrumental data, better than reanalysis. The effect is clearer in Cabo de Gata due to the directionality effect.

v. *Time series calibration.* Once the optimal calibration parameters are available, it is possible to correct the reanalysis time series related to a given location, i.e. using all data pairs. In Figure 10 the quantile-quantile plots instrumental versus reanalysis and calibrated data are shown. Note that the calibrated data shows very good diagnostics with points close to the diagonal. It is worth mentioning how the different calibration procedure works for Cabo the Gata location, where quantiles proceeding from E-ENE and W-WSW need a completely different correction, which is achieved using the proposed methodology. Note the calibrated time series presents better agreement with instrumental data, which is in most cases within the 95% confidence bands (see Figure 11).

Note that in order to gauge the added benefit of the directional correction approach, in Figure 10 it is also shown the quantile-quantile plot (green dots) associated with a nondirectional simple regression model of the form $f(\mathbf{x}; \boldsymbol{\beta}) = f(a^R, b^R; H_s^R) = a^R [H_s^R]^{b^R} = H_s^C$, where a^R and b^R are the corresponding regression parameters. In both locations the model including directional information provides results which are closer to instrumental data. This effect is stronger for Cabo de Gata, where there are two clear different wave families (“levantes” and “ponientes”) which require a different correction. Table 6 provides the relative errors of directional calibrated and nondirectional calibrated data with respect to instrumental data, respectively. Note that errors

related to the directional approach are comparatively lower for all sample moments. These results demonstrate the improvement achieved including directional information.

vi. *Diagnostic time series analysis calibration.* Using also standard regression techniques confidence intervals for the calibrated times series are calculated. This diagnostic allows quantifying the uncertainty associated with the calibration procedure. In Figure 11 the time series evolution of instrumental, reanalysis, and calibrated data is shown. Note that the calibrated time series is closer to the instrumental data improving wave climate characterization.

Finally, in Table 3 the sample distribution moments: mean (μ), standard deviation (σ), skewness (γ), and kurtosis (ξ) for reanalysis, calibrated and instrumental data are given. Note that the relative errors with respect to instrumental data for the calibrated time series are considerably lower than those for the reanalysis case. This occurs for all sample moments, which shows the good performance of the proposed procedure.

4. Analysis of Directional Uncertainty

In order to further investigate the influence of directional bias, we have performed additional tests using the instrumental directional information from both locations. Note that the calibration results shown previously in the paper contain both buoy and satellite information, we have 10404 and 12938 data pairs for Cabo de Gata and Estaca de Bares, respectively. From those data pairs, 8555 and 11737, respectively, correspond to buoy data

where instrumental directional information is available. Using these two new sets, we performed the following tests:

- i. For both locations, we perform the calibration procedure using both reanalysis and instrumental directional information, and compare the different diagnostic statistics and sample distribution moments.
- ii. In order to obtain statistically sound conclusions, and due to the linear relationship between reanalysis and instrumental directional information at Estaca de Bares location, we perform a simulation test with 1000 samples where directional information were simulated from the regression equation between reanalysis and instrumental directional data.

In Table 4 the sample distribution moments: mean (μ), standard deviation (σ), skewness (γ), and kurtosis (ξ) for reanalysis, calibrated and instrumental data considering both reanalysis (θ^R) and instrumental (θ^I) directional information are given. Note that the relative errors with respect to instrumental data for the calibrated time series are considerably lower than those for the reanalysis case. This occurs for all sample moments and using both reanalysis and instrumental directional information, which shows the good performance of the proposed procedure and its robustness with respect to possible bias in directional reanalysis data. This conclusion is further reinforced by the results shown in Table 5, where different diagnostic statistics are provided. Note that calibrated diagnostics using both directional data presents better results with respect to reanalysis data without any correction. However, no clear conclusion can be withdrawn about whether it is better to use reanalysis or instrumental directional data.

In an attempt to obtain statistically sound conclusions, we perform a simulation experiment consisting on the calibration at Estaca de Bares location using simulated directional data. A linear regression model between instrumental and reanalysis directional data is fitted, where original pairs (θ^R, θ^I) are transformed to $(\hat{\theta}^R, \hat{\theta}^I)$ to fit a unique model $\hat{\theta}^I = p_1 \hat{\theta}^R + p_2 + \epsilon$. Parameter estimates and 95% confidence intervals $p_1 = 0.9433(0.9331, 0.9535)$ and $p_2 = 25.82^\circ(22.58^\circ, 29.06^\circ)$ are obtained using least squares method. The residuals standard deviation is $\sigma = 24.43^\circ$. This model is used to generate 1000 random samples of “calibrated” reanalysis directional information, which are used within the calibration process.

In Figure 12 the sample distribution moments: (a) mean (μ), (b) standard deviation (σ), (c) skewness (γ), and (d) kurtosis (ξ) obtained during the simulation process are shown. The histogram represents the statistical distribution of each calibration sample, the light gray line corresponds to the normal fit, and the different dots represent the statistics for: (i) the calibration using reanalysis directional data (black circle dot), (ii) the calibration using instrumental directional data (square black dot), (iii) reanalysis data without calibration (asterisk black dot), (iv) instrumental data (diamond black dot), and finally (v) the mean value from simulated samples (circle light gray dot). In addition, the mean and standard deviation from simulated samples for each sample moment are shown, including also the probability of obtaining a simulated sample moment worst than the reanalysis data with respect to the instrumental data. Note that in all simulated cases the moments obtained from calibrated data are closer to instrumental moments than reanalysis data, and the probabilities of obtaining worst results with respect to reanalysis data is almost negligible. This proves the robustness of the calibration procedure with respect to uncertainty in the

directional information.

Analogous results than those in Figure 12 are given in Figure 13 for the (a) bias, (b) Pearson's correlation coefficient (ρ), (c) residual scatter index (RSI), and (d) root mean square error (RMS). Note that for all statistics but for Pearson's correlation coefficient results are always better with respect to reanalysis data, confirming the robustness of the proposed procedure. However, there is a 14.11% probability that calibration provide worst results in Pearson's correlation coefficient with respect to reanalysis.

Finally, in Figure 14 the empirical long-term distribution function of (i) calibrated data using reanalysis directional data (dashed line), (ii) calibrated data using instrumental directional data (dash-dot line), (iii) reanalysis data without calibration (dark gray line), (iv) instrumental data (black line), and finally (v) calibrated data from simulated samples (light gray lines) are shown. They are plotted in Gumbel scale. These representations allow to better check the behavior in the right tail of the distributions, which is more relevant from the engineering point of view. Note that in all cases the calibrated distributions are closer to the instrumental distribution than the reanalysis one. This reinforce the good performance of the proposed methodology.

5. Conclusions

This paper presents a calibration procedure for wave hindcast and reanalysis, which allows to make corrections based on instrumental information and considering the significant wave height direction of propagation. From the analysis reported in this paper, the following conclusions are in order:

- i. The parameter estimates for the proposed nonlinear correction model are obtained solving a mathematical programming problem, for which computationally efficient algorithms exist.
- ii. The parameters of the model vary smoothly for different directions using spline curves.
- iii. The method transforms the reanalysis database empirical distribution function to get closer to the empirical distribution function of the instrumental data. Since data belonging to the upper tail of the distribution are more relevant for design, the parameter estimates are obtained through quantiles on a Gumbel scale.
- iv. Confidence intervals for diagnostic analysis are also provided.
- v. Despite of the additional complexity inherent in the proposed calibration method with respect to traditional regression techniques, the improvement achieved makes the effort worthy.

The calibration process has been tested on different locations around Spain, correcting significant wave heights using satellite and buoy data records. Diagnostic analysis and the study of directional uncertainty show the good performance and robustness of the calibration procedure. Note that although the calibration method has only been applied to significant wave height hindcasts, the methodology seems promising to be extended and used with any other geophysical variable which includes directional information, for instance, wind velocities.

Note also that though the calibration procedure improves results, there are still discrepancies between calibrated and instrumental data, which can not be filtered with the

directional calibration. Numerical reanalysis data present less variability in the hourly scale than buoy data records, this is clearly shown in Figure 6. The main reasons are i) the spatial and temporal smoothing that all numerical wave prediction results are being through, and ii) that the spatial resolution is not enough to model the physical processes affecting high frequency waves, which may be important specially for extreme value analysis. An additional correction trying to account for high frequency waves is a subject for further research.

Another subject for further research is the applicability of the proposed methodology on a global scale. This will probably restrict the analysis to satellite information and it would require an automatic and easy to use criterion for preliminary data selection. However, we expect that this will also enhance the quality of global reanalysis databases in a near future.

Acknowledgments.

The authors would like to thank “Puertos del Estado” (Spanish State Port) for providing the information from the wave reanalysis data base. R. Mínguez is indebted to the Spanish Ministry MICINN for the funding provided within the “Ramon y Cajal” program. This work was partly funded by projects “GRACCIE” (CSD2007-00067, Programa Consolider-Ingenio 2010) and “AMVAR” (CTM2010-15009) from Spanish Ministry MICINN, by project C3E (200800050084091) from the Spanish Ministry MAMRM and by project MARUCA (E17/08) from the Spanish Ministry MF.

APPENDIX

Constrains for cubic spline definition

For the correct definition of problem (7)-(10) constraints for the evaluation of the cubic spline parameters $x_j^a, y_j^a, z_j^a, x_j^b, y_j^b, z_j^b$; $j = 1, \dots, n_p$ are required. These equations are defined using continuity conditions on the union between consecutive cubic polynomials: i) zero order (no gap exists), ii) first order derivatives, and iii) second order derivatives.

Using these conditions and once the parameter values a_j, b_j ; $j = 1, \dots, n$ are known, parameters y^a are obtained solving the following tridiagonal linear system of equations:

$$\begin{bmatrix} 2h_1 & h_1 & 0 & 0 & \cdots & 0 \\ h_1 & 2(h_1 + h_2) & h_2 & 0 & \cdots & 0 \\ 0 & h_2 & 2(h_2 + h_3) & h_3 & \cdots & 0 \\ \vdots & \vdots & \ddots & \ddots & \vdots & \vdots \\ 0 & \cdots & 0 & h_{n-1}2(h_{n-1} + h_n) & h_n & \\ 0 & \cdots & 0 & 0 & h_n & 2h_n \end{bmatrix} \begin{bmatrix} y_1^a \\ y_2^a \\ y_3^a \\ \vdots \\ y_n^a \\ y_{n+1}^a \end{bmatrix} = 3 \begin{bmatrix} \left(\frac{a_2 - a_1}{2h_1} - \frac{a_{n+1} - a_n}{2h_n} \right) \\ \left(\frac{a_3 - a_2}{h_2} - \frac{a_2 - a_1}{h_1} \right) \\ \left(\frac{a_4 - a_3}{h_3} - \frac{a_3 - a_2}{h_2} \right) \\ \vdots \\ \left(\frac{a_{n+1} - a_n}{h_n} - \frac{a_n - a_{n-1}}{h_{n-1}} \right) \\ \left(\frac{a_2 - a_1}{2h_1} - \frac{a_{n+1} - a_n}{2h_n} \right) \end{bmatrix}, \quad (\text{A1})$$

which implicitly considers that the first and second derivatives at the beginning ($\theta_1 = 0$) and at the end ($\theta_{n+1} = 2\pi$) of the spline are equal. Analogously, parameters y^b can be obtained replacing index a by b in (A1).

Once y^a parameters are known, parameters x_j^a and z_j^a can be calculated straightforwardly using the following expressions:

$$\begin{aligned} x_j^a &= \frac{1}{h_j}(a_{j+1} - a_j) - \frac{h_j}{3}(2y_j^a + y_{j+1}^a); \quad j = 1, \dots, n \\ z_j^a &= \frac{y_{j+1}^a - y_j^a}{3h_j}; \quad j = 1, \dots, n. \end{aligned} \quad (\text{A2})$$

Analogously, parameters x_j^b and z_j^b can be obtained replacing index a by b in expression (A2).

REFERENCES

- Brooke, A., D. Kendrick, A. Meeraus, and R. Raman, 1998: *GAMS: A user's guide*. GAMS Development Corporation, Washington.
- Caires, S. and A. Sterl, 2005: A new non-parametric method to correct model data: Application to significant wave height from the ERA-40 reanalysis. *Journal of Atmospheric and Oceanic Technology*, **22**, 443–459.
- Cavaleri, L. and L. Bertotti, 2004: Accuracy of the modelled wind and wave fields in enclosed seas. *Tellus*, **56A**, 167–175.
- Cavaleri, L. and M. Sclavo, 2006: The calibration of wind and wave model data in the mediterranean sea. *Coastal Engineering*, **53**, 613–627.
- Cavaleri, L., et al., 2007: Wave modelling. The state of the art. *Progress in Oceanography*, **75** (4), 603–674, doi:10.1016/j.pocean.2007.05.005.
- Crosby, D. S., L. C. Breaker, and W. H. Gemmill, 2003: A proposed definition for vector correlation in geophysics: Theory and application. *Journal of Atmospheric and Oceanic Technology*, **10**, 355–367.
- Feng, H., D. Vandermark, Y. Quilfen, B. Chapron, and B. Beckley, 2006: Assessment of wind forcing impact on a global wind-wave model using topex altimeter. **33** (11–12), 1431–1461.

- Hasselmann, S., et al., 1988: The WAM model: a third generation ocean wave prediction model. *Journal of Physical Oceanography*, **18** (12), 1775–1810.
- Hemer, M. A., J. A. Church, and J. R. Hunter, 2010: Variability and trends in the directional wave climate of the southern hemisphere. *Int. J. Climatol.*, **30** (4), 475–491.
- Jacob, D., et al., 2001: A comprehensive model intercomparison study investigating the water budget during the BALTEX-PIDCAP period. *Meteorology and Atmospheric Physics*, **77** (1–4), 19–43.
- Krogstad, H. E. and S. F. Barstow, 1999: Satellite wave measurements for coastal engineering applications. *Coastal Engineering*, **37**, 283–307.
- Lehmann, E. L. and G. Casella, 1998: *Theory of Point Estimation*. 2d ed., Springer Text in Statistics, Springer, New York.
- Mackay, E. B. L., A. S. Hahaj, and P. G. Challenor, 2010a: Uncertainty in wave energy resource assessment. Part 1: Historic data. *Renewable Energy*, **35**, 1792–1808.
- Mackay, E. B. L., A. S. Hahaj, and P. G. Challenor, 2010b: Uncertainty in wave energy resource assessment. Part 2: Variability and predictability. *Renewable Energy*, **35**, 1809–1819.
- Murtagh, B. A. and M. A. Saunders, 1978: Large-scale linearly constrained optimization. *Mathematical Programming*, **14**, 41–72.
- Murtagh, B. A. and M. A. Saunders, 1998: MINOS 5.5 Users Guide. Report SOL 83-20R SOL 83-20R, Department of Operations Research, Stanford University, Stanford, California.

- Powell, M. J. D., 1978: *Numerical Analysis*, Lecture Notes in Mathematics, Vol. 630, chap. A Fast Algorithm for Nonlinearly Constrained Optimization Calculations. Springer Verlag.
- Tomás, A., 2009: Metodologías de calibración de bases de datos de reanálisis de clima marítimo. Ph.D. thesis, Departamento de Ciencias y Técnicas del Agua y del Medio Ambiente, Universidad de Cantabria, ISBN: 978-84-693-5541-1 (in spanish).
- Tomás, A., F. J. Méndez, and I. J. Losada, 2008: A method for spatial calibration of wave hindcast data bases. *Continental Shelf Research*, **28**, 391–398.
- Wolfe, P., 1963: Methods of nonlinear programming. *Recent Advances in Mathematical Programming*, R. L. Graves and P. Wolfe, Eds., McGraw-Hill, New York, 76–77.

List of Tables

- 1 Optimal estimated parameters for both locations and 95% confidence intervals. 36
- 2 Comparison of the diagnostic statistics between reanalysis-instrumental and calibrated-instrumental for both locations. 37
- 3 Sample distribution moments (mean, standard deviation, skewness and kurtosis) and comparison between reanalysis-instrumental and calibrated-instrumental for both locations. 38
- 4 Sample distribution moments (mean, standard deviation, skewness and kurtosis) and comparison between reanalysis-instrumental and calibrated-instrumental for both locations using instrumental and reanalysis directional information. 39
- 5 Comparison of the diagnostic statistics between reanalysis-instrumental and calibrated-instrumental for both locations using instrumental and reanalysis directional information. 40
- 6 Comparison of the sample distribution moment errors between directional calibrated and nondirectional calibrated data with respect to instrumental data, respectively, at both locations. 41

TABLE 1. Optimal estimated parameters for both locations and 95% confidence intervals.

$\theta(^{\circ})$	j	Cabo de Gata						Estaca de Bares					
		a_j	a_j^{lo}	a_j^{up}	b_j	b_j^{lo}	b_j^{up}	a_j	a_j^{lo}	a_j^{up}	b_j	b_j^{lo}	b_j^{up}
0	1	1.756	1.736	1.776	0.864	0.844	0.884	1.016	1.001	1.032	1.008	0.998	1.019
22.5	2	1.734	1.713	1.756	0.847	0.827	0.867	0.809	0.791	0.827	1.214	1.197	1.230
45	3	1.413	1.396	1.431	0.741	0.728	0.754	0.943	0.925	0.962	1.068	1.053	1.084
67.5	4	1.312	1.293	1.330	0.824	0.812	0.835	1.019	1.001	1.038	0.929	0.915	0.943
90	5	1.294	1.276	1.312	0.840	0.824	0.855	0.805	0.786	0.823	1.178	1.157	1.200
112.5	6	2.304	2.253	2.355	1.047	1.016	1.078	0.748	0.727	0.769	1.199	1.175	1.222
135	7	2.811	2.728	2.894	1.467	1.416	1.518	0.738	0.718	0.759	1.166	1.144	1.189
157.5	8	2.213	2.154	2.271	1.220	1.175	1.265	0.720	0.701	0.739	1.153	1.133	1.173
180	9	1.990	1.945	2.036	1.162	1.118	1.206	0.702	0.684	0.720	1.137	1.119	1.156
202.5	10	1.854	1.819	1.889	1.173	1.132	1.213	0.693	0.674	0.712	1.129	1.109	1.148
225	11	1.852	1.834	1.871	1.048	1.029	1.067	0.665	0.646	0.683	1.123	1.105	1.141
247.5	12	1.895	1.876	1.913	0.856	0.844	0.869	0.787	0.773	0.800	1.075	1.065	1.085
270	13	1.951	1.934	1.968	0.893	0.879	0.906	0.950	0.934	0.967	0.974	0.965	0.982
292.5	14	1.930	1.912	1.948	0.946	0.928	0.965	1.039	1.023	1.054	0.950	0.943	0.958
315	15	1.880	1.862	1.898	0.907	0.888	0.925	1.018	1.003	1.033	0.964	0.957	0.971
337.5	16	1.840	1.821	1.859	0.899	0.880	0.918	1.064	1.047	1.080	0.930	0.922	0.939
360	17	1.756	1.736	1.776	0.864	0.844	0.884	1.016	1.001	1.032	1.008	0.998	1.019

TABLE 2. Comparison of the diagnostic statistics between reanalysis-instrumental and calibrated-instrumental for both locations.

	Cabo de Gata		Estaca de Bares	
	$H_s^R - H_s^I$	$H_s^C - H_s^I$	$H_s^R - H_s^I$	$H_s^C - H_s^I$
BIAS	0.3383	-0.0587	-0.0885	-0.0014
ρ	0.7165	0.7941	0.9157	0.9157
RSI	0.5835	0.4295	0.2381	0.2215
RMS	0.5922	0.4359	0.5860	0.5452

TABLE 3. Sample distribution moments (mean, standard deviation, skewness and kurtosis) and comparison between reanalysis-instrumental and calibrated-instrumental for both locations.

	Cabo de Gata			Estaca de Bares		
	H_s^R	H_s^C	H_s^I	H_s^R	H_s^C	H_s^I
Mean (μ)	0.67676	1.07376	1.01503	2.5502	2.46314	2.46170
Std. dev. (σ)	0.46948	0.64082	0.69564	1.43663	1.33066	1.36370
Skewness (γ)	2.38413	1.51797	1.51995	1.73580	1.68376	1.53668
Kurtosis (ξ)	14.69745	6.86462	6.02667	7.00561	6.79972	6.126178
ϵ (μ)	-0.33325	0.05786	–	0.03595	0.00058	–
ϵ (σ)	-0.32511	-0.07880	–	0.05349	-0.02422	–
ϵ (γ)	0.56855	-0.00130	–	0.12957	0.09571	–
ϵ (ξ)	1.43873	0.13904	–	0.14355	0.10994	–
ϵ : Relative error w.r.t. instrumental data.						

TABLE 4. Sample distribution moments (mean, standard deviation, skewness and kurtosis) and comparison between reanalysis-instrumental and calibrated-instrumental for both locations using instrumental and reanalysis directional information.

		Cabo de Gata			Estaca de Bares		
		H_s^R	H_s^C	H_s^I	H_s^R	H_s^C	H_s^I
Reanalysis θ^R	Mean (μ)	0.6476	1.0388	0.9715	2.5244	2.4438	2.4381
	Std. dev. (σ)	0.4303	0.6176	0.6663	1.3996	1.2975	1.3327
	Skewness (γ)	1.8488	1.3536	1.4750	1.5625	1.5363	1.4058
	Kurtosis (ξ)	9.5881	5.9380	5.6953	5.9127	5.8262	5.3145
	ϵ (μ)	-0.3334	0.0693	–	0.0354	0.0024	–
	ϵ (σ)	-0.3543	-0.0730	–	0.0502	-0.0264	–
	ϵ (γ)	0.2534	-0.0823	–	0.1114	0.0928	–
	ϵ (ξ)	0.6835	0.0426	–	0.1126	0.0963	–
Instrumental θ^I	Mean (μ)	0.6476	1.0412	0.9715	2.5244	2.4568	2.4381
	Std. dev. (σ)	0.4303	0.6180	0.6663	1.3996	1.2922	1.3327
	Skewness (γ)	1.8488	1.5395	1.4750	1.5625	1.5245	1.4058
	Kurtosis (ξ)	9.5881	6.7512	5.6953	5.9127	5.7381	5.3145
	ϵ (μ)	-0.3334	0.0717	–	0.0354	0.0077	–
	ϵ (σ)	-0.3543	-0.0726	–	0.0502	-0.0304	–
	ϵ (γ)	0.2534	0.0437	–	0.1114	0.0844	–
	ϵ (ξ)	0.6835	0.1854	–	0.1126	0.0797	–
ϵ : Relative error w.r.t. instrumental data.							

TABLE 5. Comparison of the diagnostic statistics between reanalysis-instrumental and calibrated-instrumental for both locations using instrumental and reanalysis directional information.

	Cabo de Gata			Estaca de Bares		
	$H_s^R - H_s^I$	$H_s^C - H_s^I (\theta^R)$	$H_s^C - H_s^I (\theta^I)$	$H_s^R - H_s^I$	$H_s^C - H_s^I (\theta^R)$	$H_s^C - H_s^I (\theta^I)$
BIAS	0.3239	-0.0673	-0.0697	-0.0863	-0.0057	-0.0187
ρ	0.7070	0.7871	0.7856	0.9145	0.9167	0.9182
RSI	0.5900	0.4393	0.4412	0.2359	0.2206	0.2184
RMS	0.5732	0.4267	0.4286	0.5752	0.5379	0.5326

TABLE 6. Comparison of the sample distribution moment errors between directional calibrated and nondirectional calibrated data with respect to instrumental data, respectively, at both locations.

	Cabo de Gata		Estaca de Bares	
	Directional	Nondirectional	Directional	Nondirectional
$\epsilon (\mu)$	0.05786	0.195910	0.00058	-0.056081
$\epsilon (\sigma)$	-0.07880	-0.135119	-0.02422	-0.021503
$\epsilon (\gamma)$	-0.00130	-0.025939	0.09571	0.148193
$\epsilon (\xi)$	0.13904	0.284560	0.10994	0.166611

List of Figures

- 1 Smooth variations of parameters $a^R(\theta)$ and $b^R(\theta)$ depending on the wave direction: a) Polar plot, b) spline for parameter $a^R(\theta)$, and c) spline for parameter $b^R(\theta)$. 44
- 2 Data selection for the calibration procedure showing reanalysis nodes, satellite data locations and buoys. 45
- 3 Data selection for the calibration procedure: (a) Moving sector for smooth quantile evaluation, and (b) empirical distribution function for a given sector i . 46
- 4 Selected locations for the calibration study: Buoy and satellite data. 47
- 5 Diagram showing the long-term distribution of wave height and direction for the selected locations: Buoy and satellite data. 48
- 6 Validation of the Wave Reanalysis Data Base using the deep water buoy “Cabo de Gata” for year 2000. 49
- 7 Selected quantiles for parameter estimation. 50
- 8 Spline correction parameters (solid lines) and 95% confidence intervals (dashed lines) for both locations. 51
- 9 Empirical long-term distribution of selected quantiles: i) Instrumental, ii) reanalysis, and iii) calibrated. 52
- 10 Diagram showing the quantile-quantile diagnostic plots for both locations, comparing reanalysis and calibrated data versus instrumental data. 53

11	Time series evolution of the a) instrumental, b) reanalysis, and c) calibrated data, including the 95% confidence intervals (gray shadow) for the Cabo de Gata location.	54
12	Sample distribution moments: (a) mean (μ), (b) standard deviation (σ), (c) skewness (γ), and (d) kurtosis (ξ) from the simulation process.	55
13	Sample distribution statistics: (a) bias, (b) Pearson's correlation coefficient (ρ), (c) residual scatter index (RSI), and (d) root mean square error (RMS) from the simulation process.	56
14	Empirical long-term distribution of selected quantiles using different directional data for calibration at Cabo de Gata and Estaca de Bares locations.	57

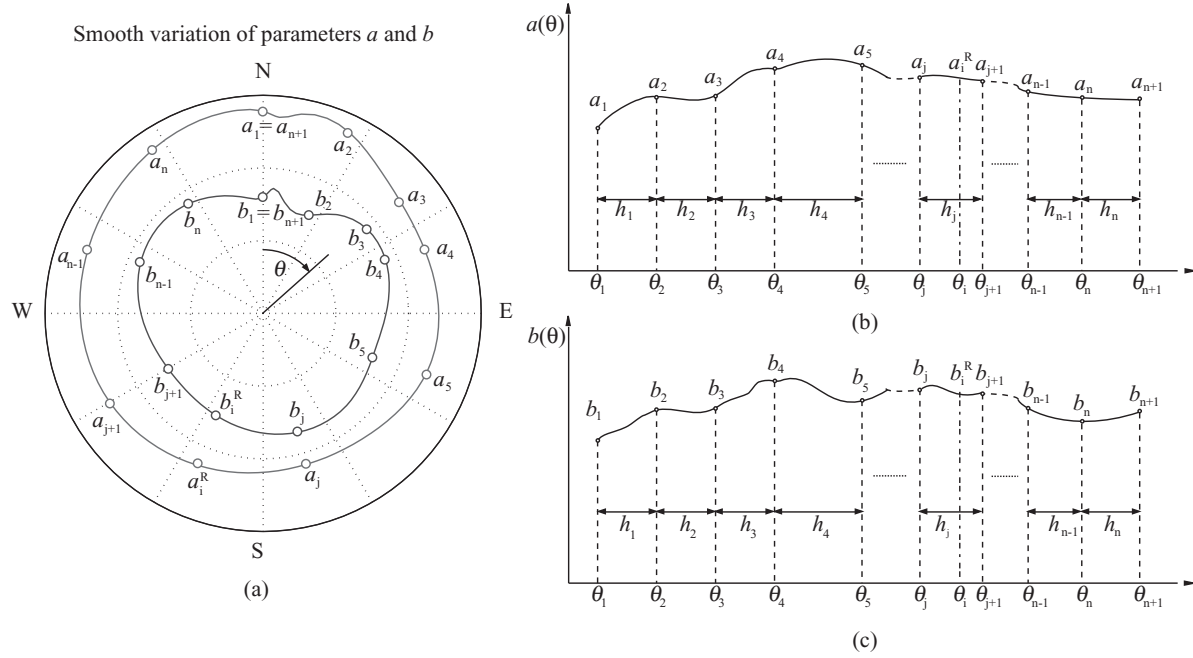


FIG. 1. Smooth variations of parameters $a^R(\theta)$ and $b^R(\theta)$ depending on the wave direction: a) Polar plot, b) spline for parameter $a^R(\theta)$, and c) spline for parameter $b^R(\theta)$.

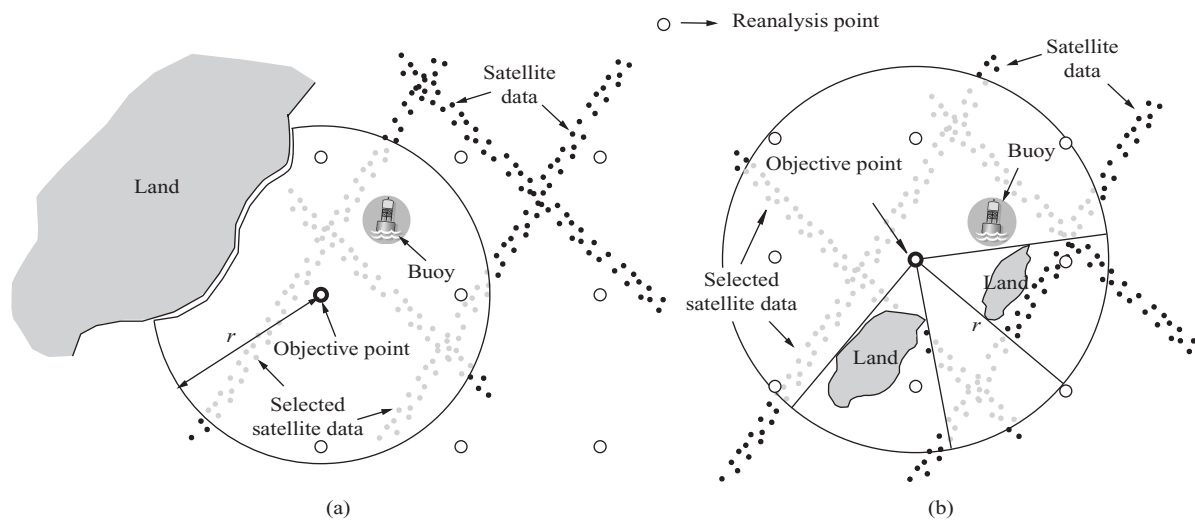


FIG. 2. Data selection for the calibration procedure showing reanalysis nodes, satellite data locations and buoys.

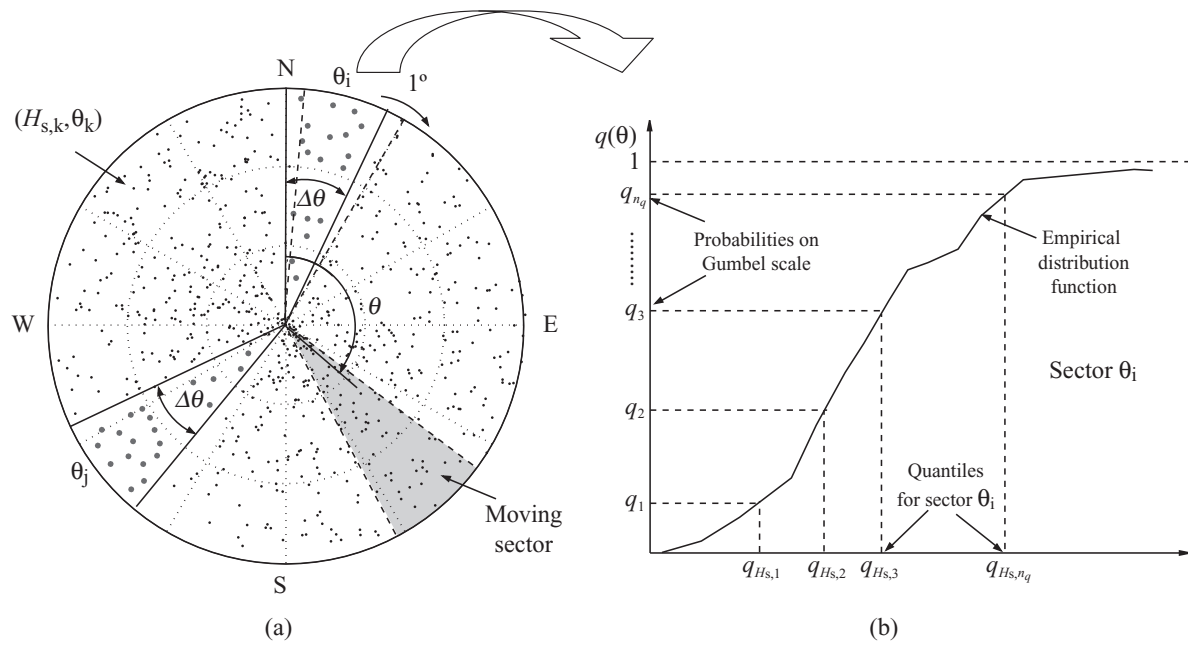


FIG. 3. Data selection for the calibration procedure: (a) Moving sector for smooth quantile evaluation, and (b) empirical distribution function for a given sector i .

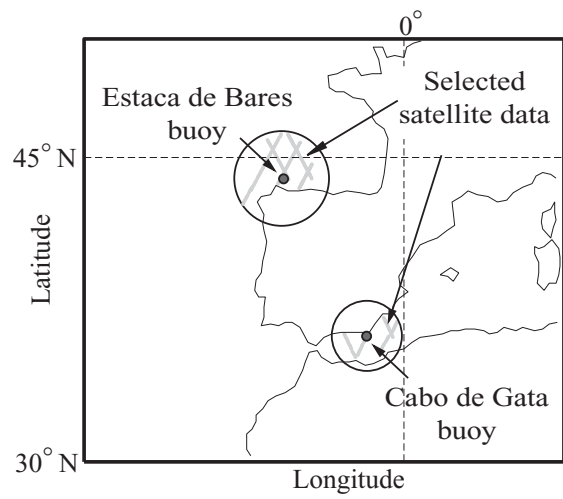


FIG. 4. Selected locations for the calibration study: Buoy and satellite data.

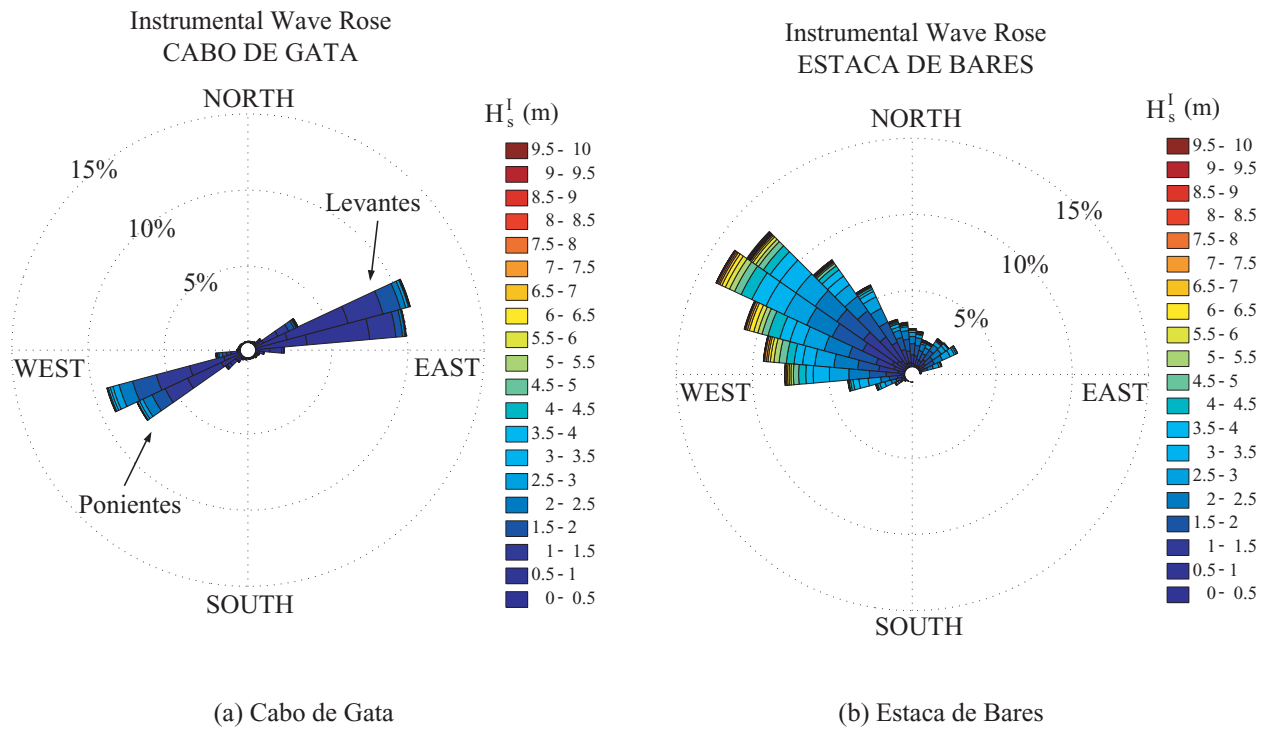


FIG. 5. Diagram showing the long-term distribution of wave height and direction for the selected locations: Buoy and satellite data.

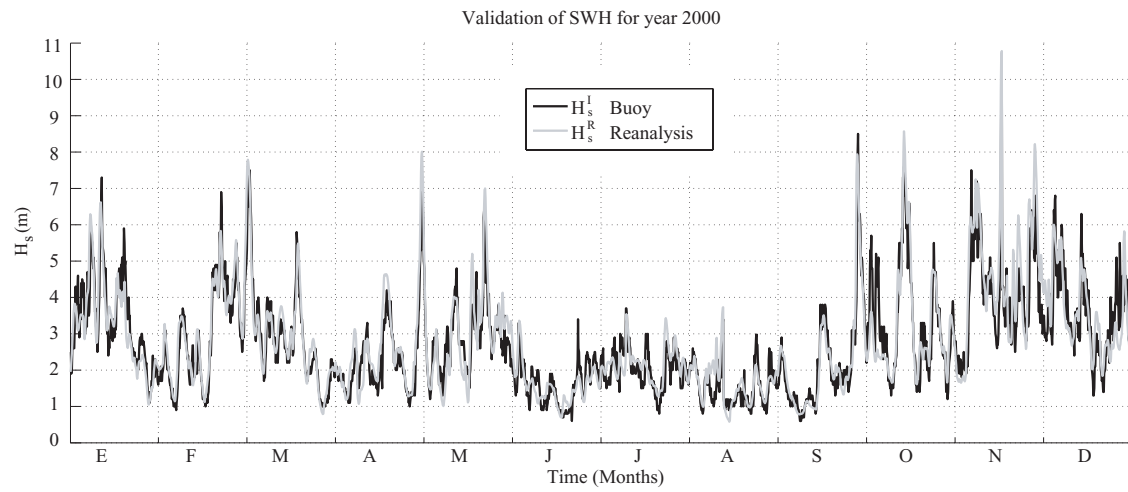


FIG. 6. Validation of the Wave Reanalysis Data Base using the deep water buoy “Cabo de Gata” for year 2000.

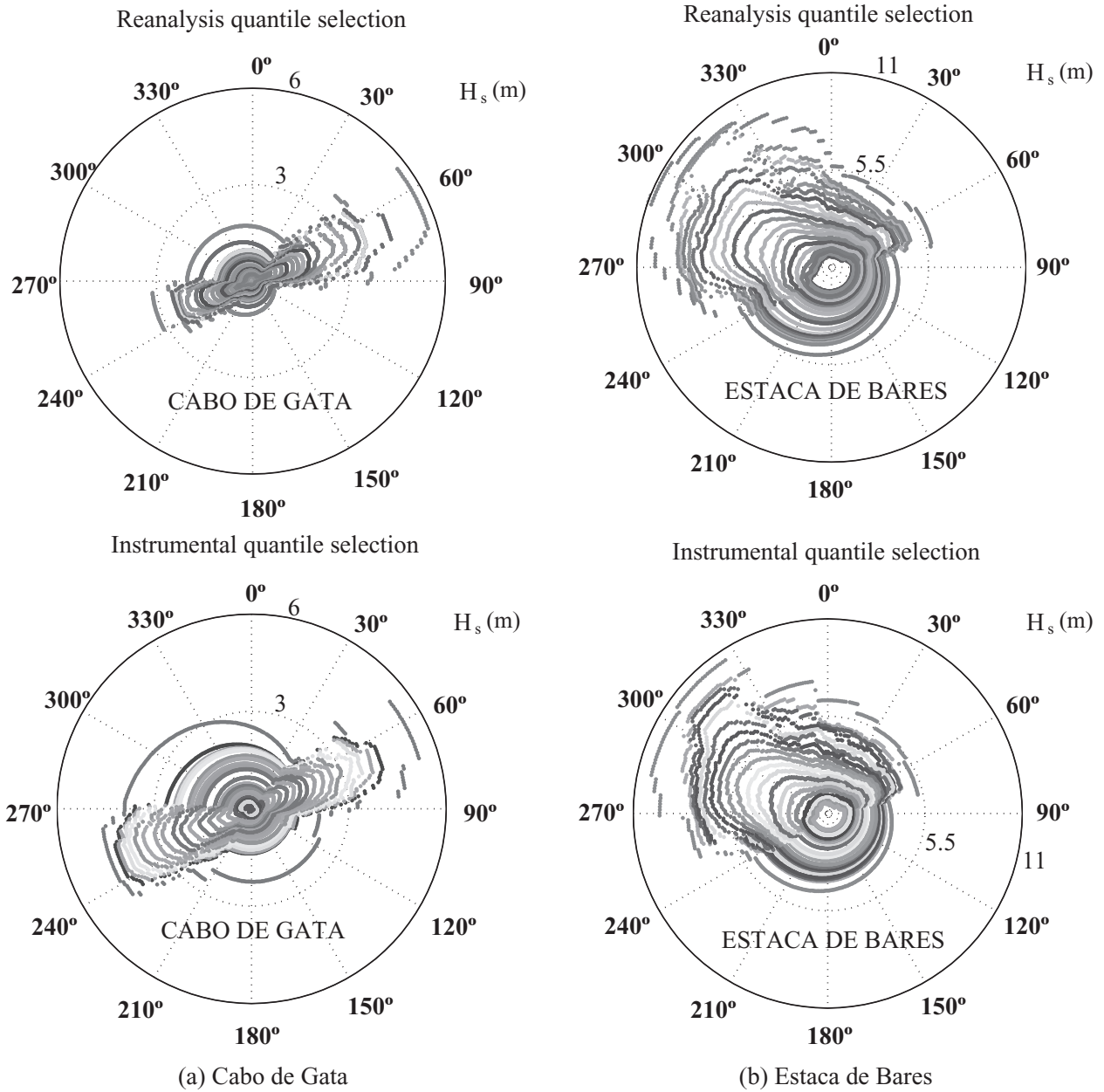


FIG. 7. Selected quantiles for parameter estimation.

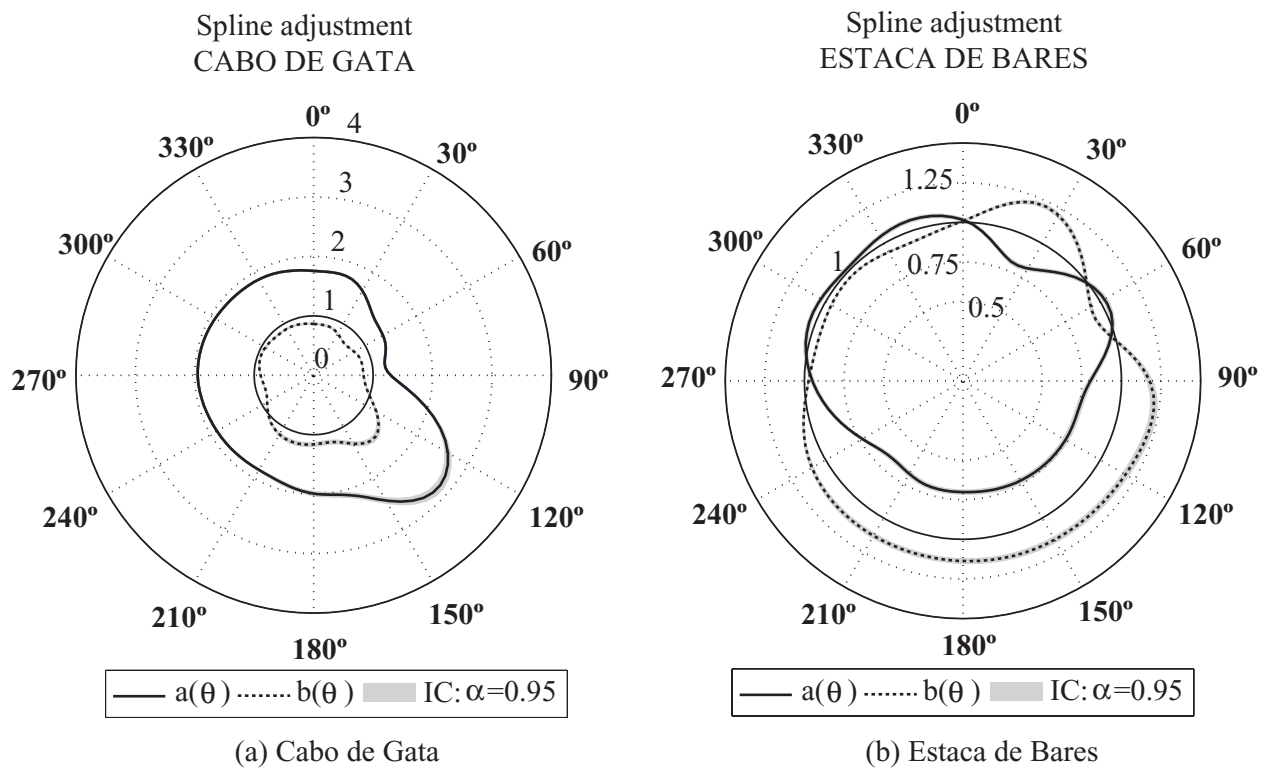


FIG. 8. Spline correction parameters (solid lines) and 95% confidence intervals (dashed lines) for both locations.

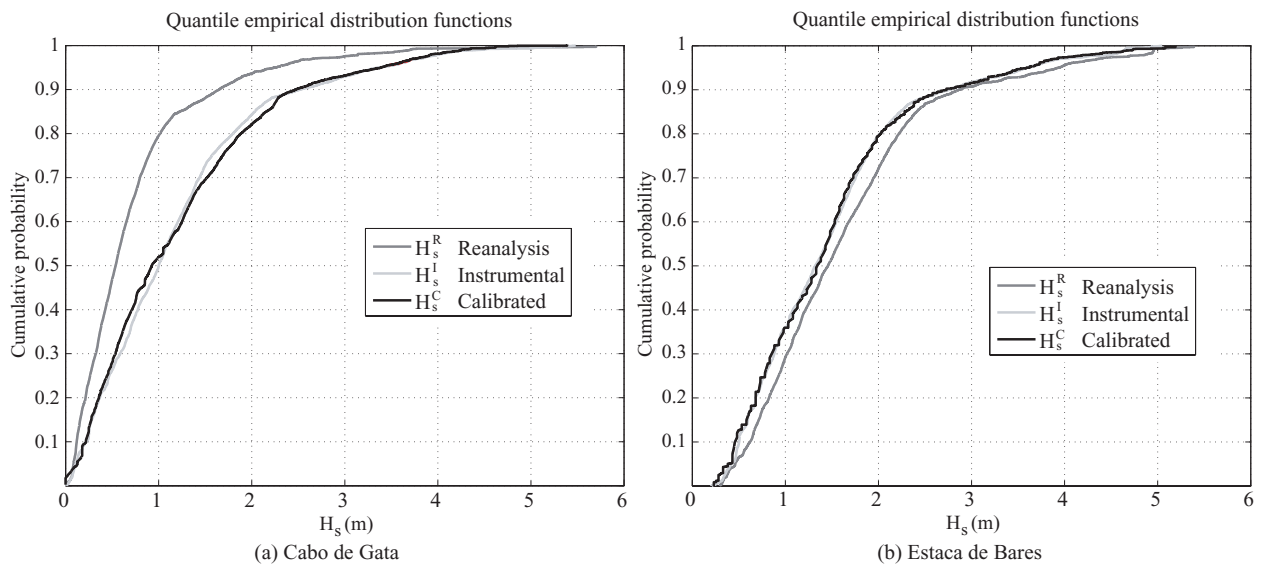


FIG. 9. Empirical long-term distribution of selected quantiles: i) Instrumental, ii) reanalysis, and iii) calibrated.

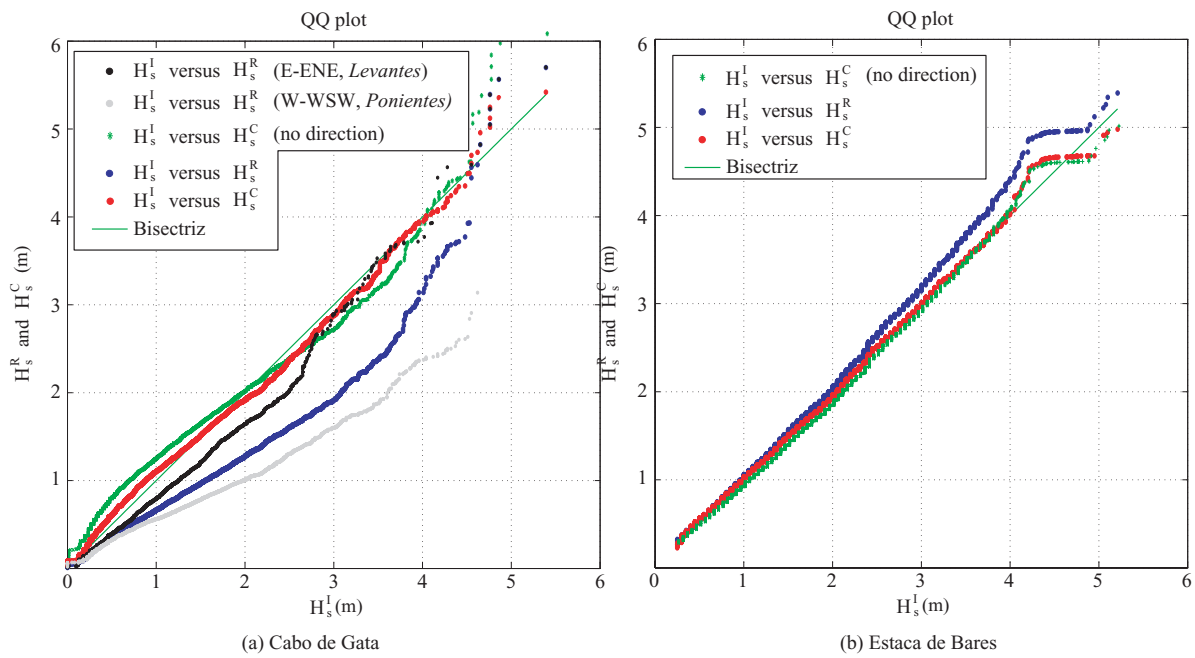


FIG. 10. Diagram showing the quantile-quantile diagnostic plots for both locations, comparing reanalysis and calibrated data versus instrumental data.

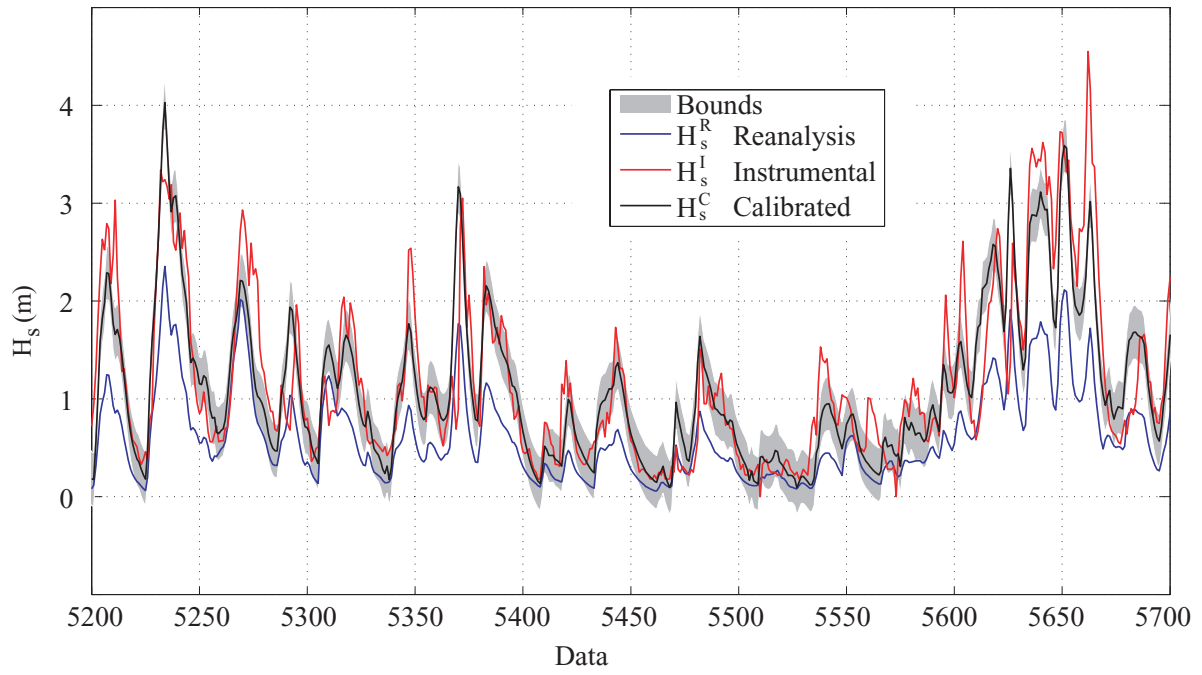


FIG. 11. Time series evolution of the a) instrumental, b) reanalysis, and c) calibrated data, including the 95% confidence intervals (gray shadow) for the Cabo de Gata location.

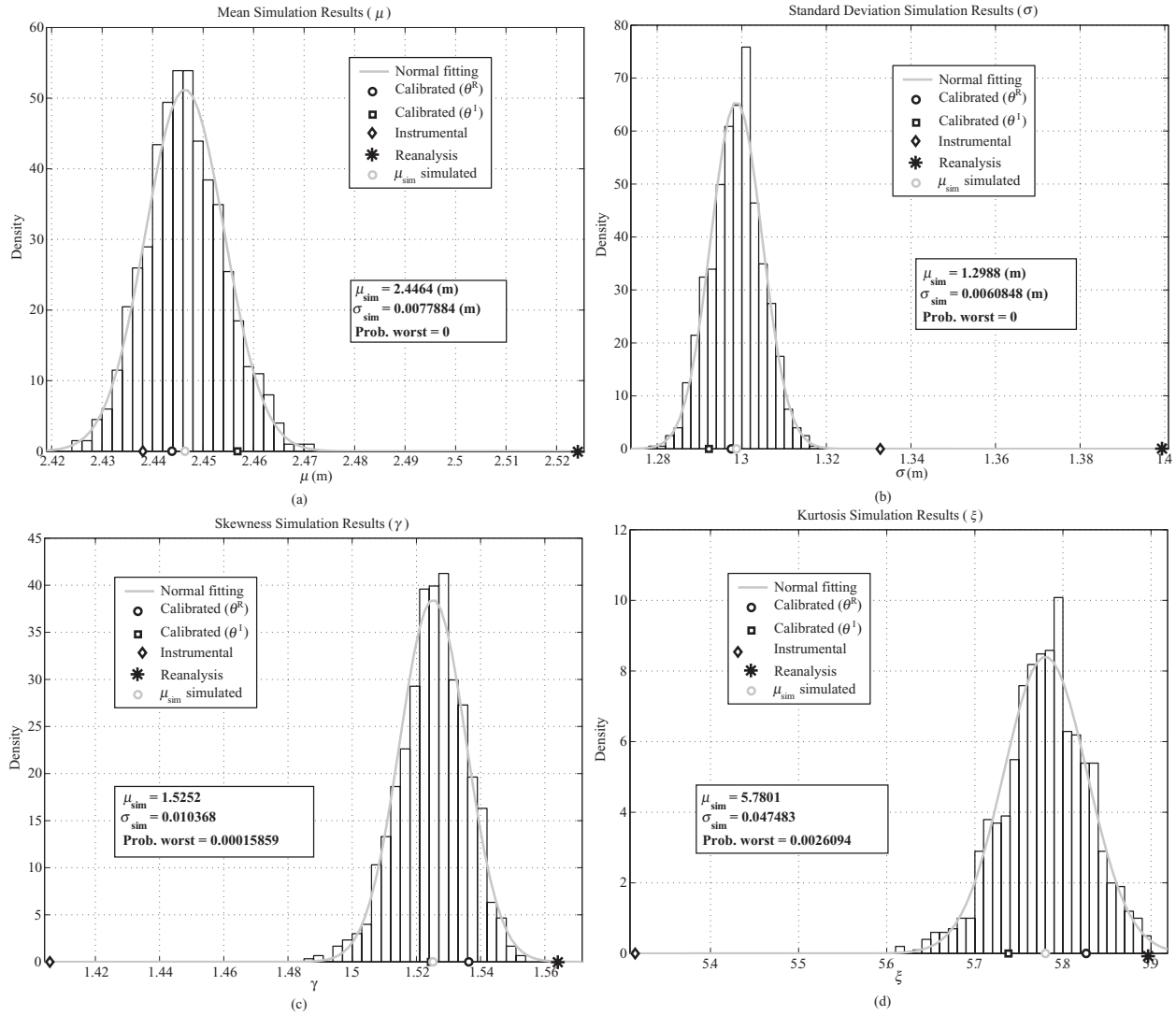


FIG. 12. Sample distribution moments: (a) mean (μ), (b) standard deviation (σ), (c) skewness (γ), and (d) kurtosis (ξ) from the simulation process.

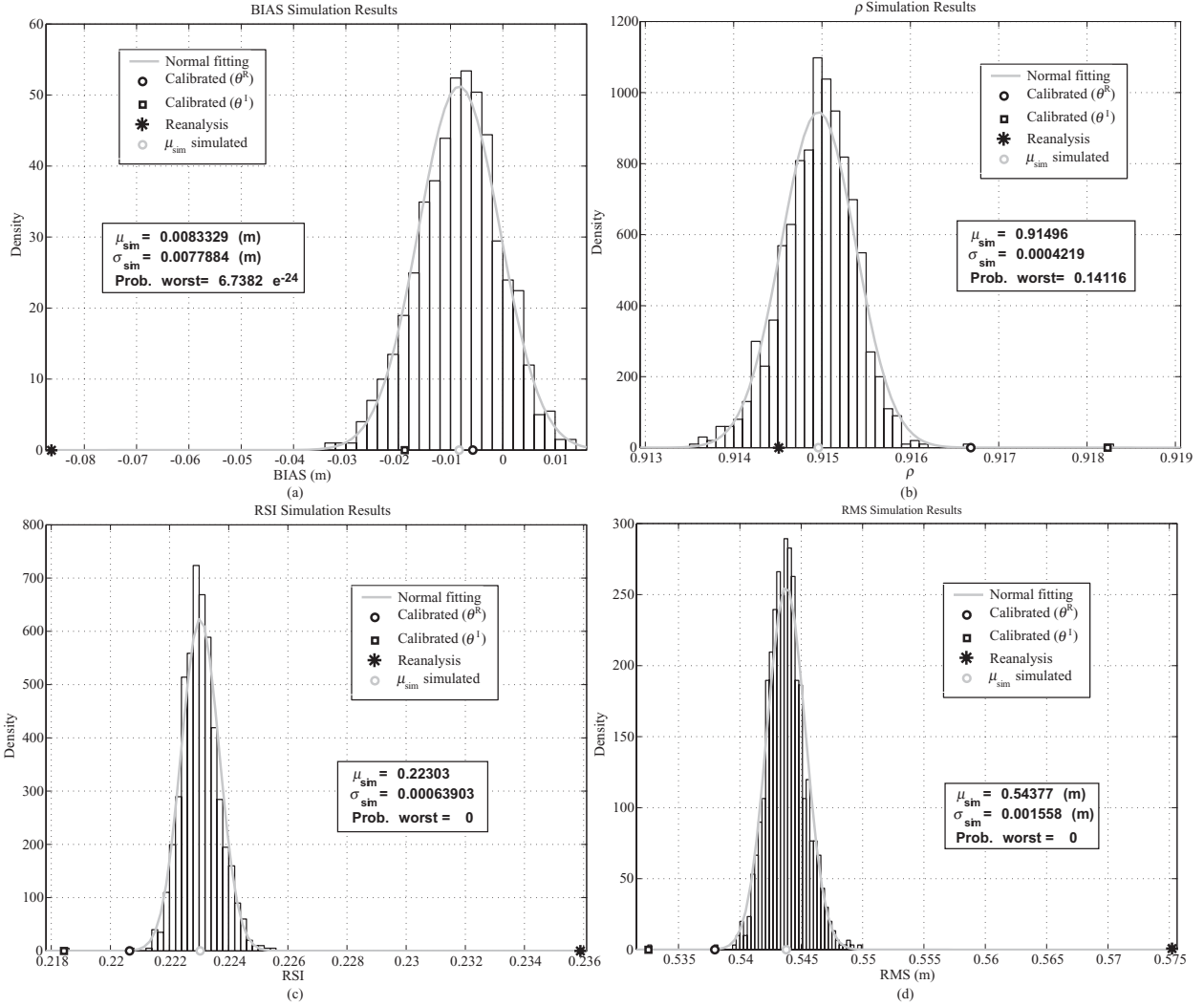


FIG. 13. Sample distribution statistics: (a) bias, (b) Pearson's correlation coefficient (ρ), (c) residual scatter index (RSI), and (d) root mean square error (RMS) from the simulation process.

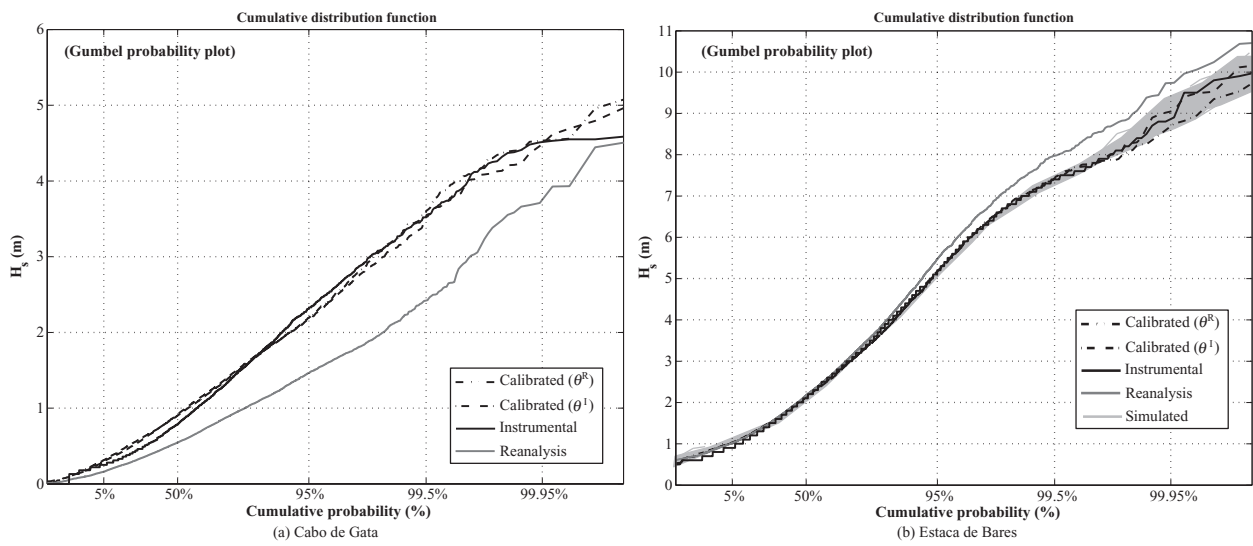


FIG. 14. Empirical long-term distribution of selected quantiles using different directional data for calibration at Cabo de Gata and Estaca de Bares locations.